Journal of Engineering Science 11(1), 2020, 123-131

JES
an international Journal

MODIFICATION IN STRUCTURAL, MORPHOLOGICAL, MAGNETIC AND FERROELECTRIC PROPERTIES OF CALCIUM-DOPED BISMUTH FERRITE NANOPARTICLES

Nushrat Naushin[1], Sadi Md. Shahriar[1*], Oishy Roy[2] and Ahmed Sharif[2]

[1]*Department of Materials Science & Engineering, Khulna University of Engineering & Technology, Khulna*
[2]*Department of Materials & Metallurgical Engineering, Bangladesh University of Engineering & Technology*

Received: 22 December 2019 Accepted: 30 May 2020

ABSTRACT

The structural, morphological, magnetic and ferroelectric properties of calcium (Ca) doped bismuth ferrite (BFO) synthesized using a sol-gel method were studied. X-ray diffraction (XRD) analysis followed by Rietveld refinement revealed the lattice distortion of BFO after doping with 6% and 8% Ca. This also led to the reduction in particle size by creating oxygen vacancies, which was observed from the surface morphology using Field Emission Scanning Electron Microscopy (FESEM). The Magnetic properties exhibited some enhancements in saturation magnetization when the particle size was near a limiting value. The reduction in the coercive magnetic field with the increase in dopant concentration was also evident from the M-H hysteresis loop measured by Vibrating Sample Magnetometer (VSM). The Ferroelectric P-E hysteresis loop exhibited an increased symmetry in the hysteresis loop and increase in the polarization with the increase in %Ca. The 8% Ca doped BFO exhibited an incomplete saturation in the hysteresis loop and was evident to exhibit leakage current characteristics.

Keywords: *Multiferroic; Nanoparticles; Morphology; XRD; Rietveld refinement; Hysteresis loop.*

1. INTRODUCTION

Multiferroic materials, exhibiting a combination of ferroelectric and ferromagnetic propertiessimultaneously, have been the subject of extensive research in recent years due to their unique physics which is suitable for potential applications in sensors, transducers, spintronics, data storage, quantum electromagnets, and electric field-controlled ferromagnetic resonance deviceetc (Fiebig *et al.,* 2002; Kimura *et al.,* 2003; Cheong *et al.,* 2007; Martin *et al.,* 2008; Catalan *et al.,* 2009; Wang *et al.,* 2009). Single-phase multiferroic materials such as $TbMnO_3$, $YMnO_3$, $BiMnO_3$ and $BiFeO_3$ have been the focus of the most studies in the last few decades (Seshadri *et al.,* 2001; Wang *et al*., 2003; Van Aken *et al.,* 2004; Xiang *et al.,* 2008; Cheng *et al.,* 2016; Manz *et al.,* 2016; Zhai *et al.,* 2017; Sayedaghaee *et al*., 2019). Among these studies, $BiFeO_3$ (BFO) is the only room temperature single-phase multiferroic (Ramesh 2014) and has a rhombohedral unit cell (space group R3c) in which two distorted perovskite cells are linked along a pseudo-cubic [111] direction. BFO has sparked a deal of interest in recent times because it's Curie temperature and Néel temperature are ~1103 K and 643 K, respectively, enabling it to display both ferroelectricity and G-type antiferromagnetism at room temperature so that room temperature applications are possible (Sosnowska *et al.,* 1982; Ederer and Spaldin, 2005; Qi *et al.*, 2005; Han *et al.,* 2014). The lone pair (s^2 orbital) of Bi^{3+} and local spin ordering of Fe^{3+} induce the polarization and antiferromagnetism of BFO, respectively. Hence, the A-site (Bi^{3+}) contributes mostly to the polarization, while the magnetization results from the B-site (Fe^{3+}). However, pure BFO is unfeasible for multifunctional applications owing to its poor electrical and magnetic properties which arise from a large leakage current, impurity phases such as $Bi_{25}FeO_{39}$ and $Bi_2Fe_4O_9$, and weak magnetoelectric coupling (Kumar and Kar, 2000; Gautam *et al.,* 2011; Bhushan *et al.,* 2012). During conventional processing of this material, it is difficult to obtain larger magnetoelectrics due to the volatilization of A-site Bi^{3+}, as the existence of the pure phase of $BiFeO_3$ delays the conversion of Fe^{3+} into Fe^{2+}. This may be due to the presence of an oxygen vacancy, which is the cause of leakage current (Lin *et al.,* 2018).

To overcome the limitations of pure BFO, researches have been carried out to enhance its ferroelectric and magnetic properties. Several studies have shown that doping the A-site in BFO with different substituents could result in decrease of oxygen vacancies and improvement of the structure and magnetoelectric properties by suppressing the volatilization of bismuth (Lee *et al.,* 2005; Yuan *et al*., 2006; Yoneda *et al*., 2007; Khomchenko *et al.,*2008; Cheng *et al.,* 2009; Troyanchuk *et al.,* 2009). A-site doping with alkaline-earth ions such as Ca^{2+} (Catalan *et al.,* 2009; Marzouk *et al.,* 2020; Tahir *et al.,* 2020), Sr^{2+} (Bhushan *et al.,* 2010; Dhir *et al.,* 2018), Ba^{2+} (Wang *et al.,* 2006; Soltani *et al.,* 2016; Makhdoom *et al.,* 2019) and rare-earth ions such as La^{3+}, Nd^{3+}, Ce^{3+} and Tb^{3+} (Huang *et al.,* 2006; Wang and Nan, 2008; Yu *et al.,* 2008; Lahmar *et al.,* 2009; Liu *et al.,* 2010; Dai *et al.,* 2016; Koval *et al.,* 2017; Yotburut *et al.,* 2017; Wang *et al.,* 2020) have mainly been studied so far. Substitution of divalent alkaline-earth ions have especially been proven effective in improving the ferroelectric

* Corresponding Author:*sadimdshahriar@mse.kuet.ac.bd*

ISSN 2075-4914 (print); ISSN 2706-6835 (online)

and ferromagnetic properties of BFO. Nanoparticles (NPs) of BFO doped with Sr exhibited typical M–H behavior of a ferromagnet with saturation magnetization attained within an applied magnetic field of 10kOe (Bhushan *et al*., 2010). Ba-doped BFO NPs also showed a great enhancement on dielectric, optical, and magnetization properties (Chauhan *et al*., 2013).

In the bulk and film form of BFO, smaller Ca^{2+} ions with a radius of 0.99 Åhave been widely used to substitute larger Bi^{3+} ions with a radius of 1.03 Å (Khomchenko *et al*., 2008; Yang *et al.,* 2009; Masó and West, 2012). According to Maso´ and West (2012), variations in the electrical conductivity of Ca-doped bulk BFO occur by several orders of magnitude depending on the oxygen partial pressure during processing. Huang *et al.* (2011) and Yang *et al.* (2009) reported that, for BFO thin film, A-site Ca-doping facilitates a transformation to tetragonal phase with higher crystal symmetry, and band filling by the doping could regulate conductor to insulator transition. However, investigations based on Ca-doped BFO NPs are rare. In addition, more than 10 mol% dopants were used in most of the works involving Ca-doped BFO. Therefore, we study the effects of the addition of a lower Ca content (6 and 8 mol%) on BFO NPs synthesized by sol-gel method in this work.

The motivation of this particular investigation is to perceive whether a small change in the composition can have significant effect in the crystallographic structures, lattice parameters, and the magnetic and ferroelectric properties of BFO. Althoughstudies like that conducted by Chauhan *et al.* (2016) used similar concentrations of Ca-doping (0 to 20% with 5% increment), we utilized a much narrower range of doping concentrations. Besides, ferroelectric analysis is absent in their work. In addition, they used tartaric acid as chelating agent in the sol-gel process whereas we used citric acid.Moreover, the stirring time and rate implemented by them is different from ours. This leads to slight variations in microstructures and properties for the same compositions.

2. EXPERIMENTAL

All the samples of pure BFO and Ca-doped BFO, $Bi_{1-x}Ca_xFeO_3$ ($x = 0.06$ and 0.08), were prepared using the sol-gel route. The starting chemicals were Bismuth Nitrate Pentahydrate (>99% pure), Ferric Nitrate Nonahydrate (>98% pure), Calcium nitrate (>99% pure), Citric Acid Monohydrate (>99% pure) and ethylene glycol. All the chemicals were manufactured by Merck, India. Equimolar amounts of the metal nitrate precursors were dissolved in deionized water and 2 molar citric acid was added. 6% excess wt. bismuth was added to compensate the loss of volatile bismuth while annealing. The mixture was simultaneously heated at 80°C and stirred at 450 rpm to form the suspension. The orange suspension is then constantly heated and stirred until the suspension turns brown and then 5 ml ethylene glycol was added as it acts as a homogenizing agent in the sol (Ahmadi *et al.,* 2017). Then the sol gradually turned into brown foamy gel which was eventually burnt out. The gel is then dried at 110ºC for 16 hours followed by crushing the dried gel into powder using agate mortar and pestle, two different heating cycles were used. At the first one, the powder was then heated at a rate of 5 °C per minute up to 500 °C, while on the other heating cycle, the maximum temperature was 550°C. The powder was calcined for two hours followed by furnace cooling. The microstructures of the powdered samples were observed using FESEM (JEOL JSM 7600F) from the Department of Glass and Ceramic Engineering, BUET, Dhaka. For further image analysis, MIPAR software was used. XRD analysis was carried out using PANalytical Empyrean X-Ray Diffractometer system) utilizing a Cu x-ray source (wavelength: =1.540598Å and =1.544426Å). For extracting crystallographic information from the obtained XRD data, Rietveld Analysis was performed using X'pertHIGHSCORE Plus. The room temperature magnetic properties were measured using the vibrating sample magnetometer (VSM: EV-9 Microsense). For analyzing the ferroelectric property, the polarization hysteresis was performed at room temperature using a frequency of 100 Hz and an electric field of 10kV/mm with the help of the ferroelectric test system (Radiant Precision Multiferroic). Prior to the test, the powdered samples were compacted in the form of tablets using 0.76g of powdered samples using a hand pressing machine. The tablets had a diameter of around 1.2cm and a thickness of 1.2mm. The tablets were then sintered using the same heat treatment cycle as the annealing operation which is the tablets are heated at the rate of 5°C/min and held at 550°C for 2 hours followed by furnace cooling. Then both of the surfaces of the tablet were covered with silver paste to create a conductive layer.

3. RESULTS AND DISCUSSION

3.1 Morphological Analysis

The FESEM micrographs were analyzed using MIPAR software. The observed images shown in Figure 1 exhibited nearly circular powder particles and the particle size increased with increasing the annealing temperature and simultaneously showed a decrease in particle size with the addition of Ca dopant. The reason behind the change in particle size is the creation of oxygen vacancies due to the substitution of Bi^{3+} by Ca^{2+}. The defect reaction (Kröger-Vink notation) representing this phenomenon is given by:

$$2Ca^{2+} \xrightarrow{2BiFeO_3} 2Ca'_{Bi} + 2Fe^{X}_{Fe} + 6O^{X}_{O} + V^{"}_{O}$$

The following reactions represent the synthesis of 6% and 8% Ca doped BFO, respectively:

$$2\times0.06\ CaO + 0.94\ Bi_2O_3 + Fe_2O_3 \rightarrow 2Bi_{0.94}Ca_{0.06}FeO_3$$

$$2\times0.08\ CaO + 0.92\ Bi_2O_3 + Fe_2O_3 \rightarrow 2Bi_{0.92}Ca_{0.08}FeO_3$$

The average particle size of $BiFeO_3$, $Bi_{0.94}Ca_{0.06}FeO_3$ and $Bi_{0.92}Ca_{0.08}FeO_3$ annealed at 550ºC were 114.8 nm, 82.57nm and 76.4 nm, respectively. And the observed average particle sizes for $BiFeO_3$, $Bi_{0.94}Ca_{0.06}FeO_3$ and $Bi_{0.92}Ca_{0.08}FeO_3$ annealed at 500ºC were 105.6 nm, 72.65 nm and 68.79 nm, respectively. The increase in particle size with increase in annealing temperature can be explained with Ostwald ripening process where the internal stress and lattice distortion result in the change in grain morphology.

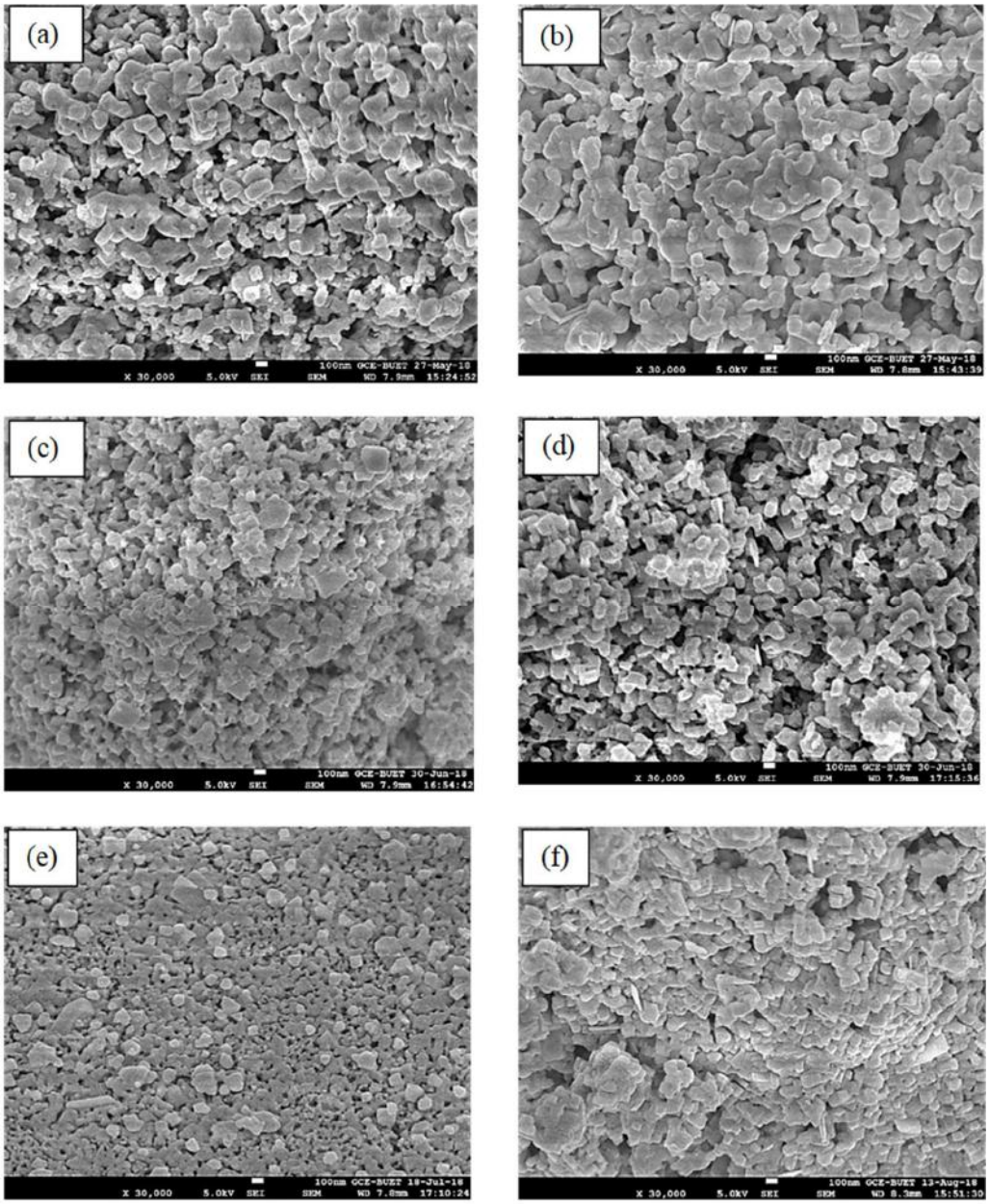

Figure 1: FESEM micrographs of Pure BFO annealed at 500°C (a) and 550°C (b); 6% Ca doped BFO annealed at 500°C (c) and 550°C (d); 8% Ca doped BFO annealed at 500°C (e) and 550°C (f) with a heating cycle including 2 hours of holding time. The magnification of each image is 30,000X.

The x-ray diffraction analysis results are exhibited in Figure 2(a), while Figure 2(b) represents the magnified XRD pattern at the range of 31-33º. All the patterns exhibited a peak of Bi_2O_3 (denoted with a 'star' sign in the pattern). The source of the Bi_2O_3 is the additional $Bi(NO_3)_3$ which was added to prevent the deficiency of Bismuth and creation of non-stoichiometric BFO. From the magnified peaks of all the samples, the peaks for (104) and (110) plane are clearly distinctive in pure BFO, while the peaks are observed to merge into a single peak for the Ca substituted BFO samples. This is because of the distortion of the crystal structure due to the substitution. The Goldschmidt tolerance factor (t) is used to quantify the structural stability of perovskite compounds (Kumar *et al.*, 2014). The tolerance factor is given by:

$$t=\frac{(<r_A>+r_o)}{\sqrt{2}\,(<r_B>+r_o)}$$

Where, r_A, r_B and r_o are the effective ionic radii of the elements A, B and oxygen, respectively in the ABO_3 perovskite compounds. A tolerance factor less than one indicates a compressive strain working on Fe-O bonds, which means a strain works on the Bi-O bond too. And all these induce lattice distortion. The tolerance factor calculated for pure BFO is 0.881163 and for $CaFeO_3$ is 0.870285. Which means the tolerance factor for the doped samples will be in between 0.881163 and 0.870285. The doping of the compound induces further distortion which is responsible for the changes in the XRD pattern of pure BFO.

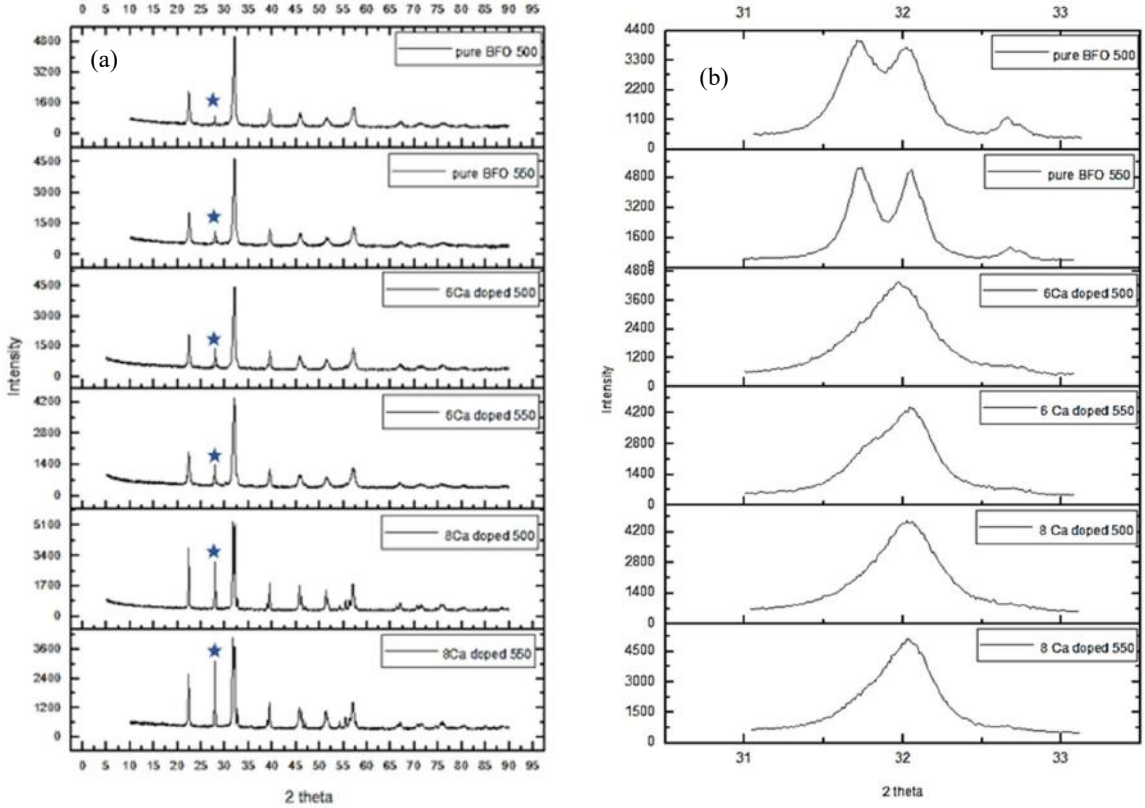

Figure 2: (a) XRD patterns of pure ($BiFeO_3$) and Ca doped Bismuth ferrite [$Bi_{1-x}Ca_xFeO_3(x = 0.06, 0.08)$] annealed at 500°C and 550°Cwith 2 hours holding time; (b) Magnified XRD pattern at the range of 31-32.99º

3.2 Structural Analysis

The Rietveld refinement of the XRD data was performed using PANalytical X'pert HIGHSCORE Plus. The R factors and the goodness of fit were determined. From figure 2(b) the pure BFO structure for x=0 clearly represents distorted rhombohedral phase in hexagonal structure exposed by the peak position in $2\theta \sim 31$ to 33°. It is also observed that the rhombohedral phase peaks get attenuated and shrunk due to Ca-doping in BFO up to x=0.06 and 0.08, and are almost diminished. The goodness of fit is between 1.11 and 1.25, which indicates the accuracy of the refinement. It was observed that the substitution of Bi^{3+} with Ca^{2+} reduces the overall lattice parameter and the volume of the ceramic. It is because Ca^{2+} has the effective ionic radius of 100 pm which is lower than the cationic radius of Bi^{3+} (103 pm). The information obtained from the Rietveld analysis is tabulated in Table 1.

Table 1: Rietveld refined structural parameters and phases fraction obtained from XRD with R_{exp} (structure factor), R_p (residual for the unweighted pattern), R_w (residual for the weighted pattern) and χ^2 (goodness of fit) and composition of the $BiFeO_3$ and $Bi_{1-x}Ca_xFeO_3$ (x=0.06 and 0.08)

Sample Identity	Crystal Structures	Lattice Parameters	R factors	χ^2 (Goodness of fit)
$BiFeO_3$ (500°C)	$BiFeO_3$: 84.5 %, Rhombohedral (ICSD 01-076-8070) Bi_2O_3:15.5 %, Tetragonal (ICSD 98-022-8443)	a=b= 5.577582 Å c=13.86545 Å α=β=90°, ϒ=120° a=b= 7.738329 Å c= 5.632214 Å α=β=ϒ= 90°	R_{exp}= 4.51725 R_p= 4.32388 R_w= 5.63222	1.25
$BiFeO_3$ (550°C)	$BiFeO_3$: 81.7%, Rhombohedral (ICSD 01-076-8070) Bi_2O_3: 18.3%, Tetragonal (ICSD 98-022-8443)	a=b= 5.57854 Å c= 13.8692 Å α=β=90°, ϒ=120° a=b= 7.738797 Å c= 5.630169 Å α=β=ϒ= 90°	R_{exp}= 4.43786 R_p= 4.37274 R_w= 5.64899	1.27
$Bi_{0.94}Ca_{0.06}FeO_3$ (500°C)	$Bi_{0.97}Ca_{0.03}FeO_3$: 42.6%, Rhombohedral (ICSD 01-081-9406) $BiFeO_3$: 48.7%, Rhombohedral (ICSD 01-080-2685) Bi_2O_3: 8.7%, Tetragonal (ICSD 98-041-7638) $Bi_{0.97}Ca_{0.03}FeO_3$: 52.6%, Rhombohedral (ICSD 01-081-9406)	a=b= 5.560684Å c= 13.82306Å α=β=90°, ϒ=120° a=b= 5.581699Å c= 13.88348 Å α=β=90°, ϒ=120° a=b= 7.740589Å c= 5.644079 Å α=β=ϒ= 90° a=b= 5.565022 Å c= 13.87912 Å α=β=90°, ϒ=120°	R_{exp}= 4.33031 R_p= 4.036 R_w= 5.19177	1.20
$Bi_{0.94}Ca_{0.06}FeO_3$ (550°C)	$BiFeO_3$: 37.3%, Rhombohedral (ICSD 01-080-2685) Bi_2O_3: 10.1%, Tetragonal (ICSD 98-041-7638) $Bi_{0.97}Ca_{0.03}FeO_3$: 51.7%, Rhombohedral (ICSD 01-081-9406)	a=b= 5.579215 Å c= 13.92983 Å α=β=90°, ϒ=120° a=b= 7.755355 Å c= 5.633923 Å α=β=ϒ= 90° a=b=5.582328 Å c= 13.75105 Å α=β=90°, ϒ=120°	R_{exp}= 4.4454 R_p= 3.95308 R_w= 5.1045	1.15
$Bi_{0.94}Ca_{0.08}FeO_3$ (500°C)	$BiFeO_3$: 38.9 %, Rhombohedral (ICSD 01-080-2685) Bi_2O_3: 9.4 %, Tetragonal (ICSD 98-041-7638) $Bi_{0.97}Ca_{0.03}FeO_3$: 46.8%, Rhombohedral (ICSD 01-081-9406)	a=b= 5.605713 Å c= 13.86102 Å α=β=90°, ϒ=120° a=b=7.761659 Å c= 5.640444 Å α=β=ϒ= 90° a=b= 5.576849 Å c= 13.74126 Å α=β=90°, ϒ=120°	R_{exp}= 4.2271 R_p= 3.66267 R_w= 4.7067	1.11
$Bi_{0.92}Ca_{0.08}FeO_3$ (550°C)	$BiFeO_3$: 47.7%, Rhombohedral (ICSD 01-077-5214) Bi_2O_3: 5.5%, Tetragonal (ICSD 98-018-9995)	a=b= 5.594097 Å c= 13.84153 Å α=β=90°, ϒ=120° a=b= 7.748043 Å c= 5.631373 Å α=β=ϒ= 90°	R_{exp}= 4.33031 R_p= 4.036 R_w= 5.19177	1.20

3.3 Measurement of Magnetization

VSM: EV-9 Microsense was used to construct the magnetization versus magnetic field diagram for the prepared samples which were annealed at 550ºC as shown in Figure 3. To know the ferromagnetic effect on BFO and Ca

doped BFO, the full cycle M-H curve was obtained up to a maximum applied field of 10 kOe. The remnant magnetization is found to be 0.88 emu/g for pure $BiFeO_3$. This is due to the fact that BFO naturally shows antiferromagnetic property which is among few unusual ferromagnetic behaviors. The coercive magnetic field (H_c) is observed to decrease with the substitution of Bi with Ca. The H_c further decreases with increasing the %Ca. The remnant magnetization and saturation magnetization are observed to decrease when doped with 6% Ca, but then increases with increasing the %Ca. The increase in coercive magnetic field with increasing dopant concentration can be explained from the size reduction in the particles from the SEM micrographs (Pattanayak *et al.,* 2013). According to Wang *et al.* (2015), magnetic property may increase due to the size effect, as it gives rise to the suppression of spin spiral ordering structure in a condition that the size of the nanoparticle is below the periodicity of spin helical ordering structure (62nm). This explains the increase in remnant and saturation magnetization when the %Ca increases. It can be depicted from the observed data for pure BFO and 6% Ca doped BFO that, this effect does not work for a higher size of nanoparticles. The ferromagnetic properties of pure and Ca-doped BFO as determined from the graph manually are summarized in Table 2.

Table 2: Ferromagnetic properties of pure and Ca-doped BFO

Sample Identity	Coercivity H_c(Oe)	Remnant Magnetization M_r (emu/g)	Saturation Magnetization M_s (emu/g)
$BiFeO_3$	180.469	0.88	3.33
$Bi_{0.94}Ca_{0.06}FeO_3$	122.142	0.26	1.63
$Bi_{0.92}Ca_{0.08}FeO_3$	82.89	0.23	1.997

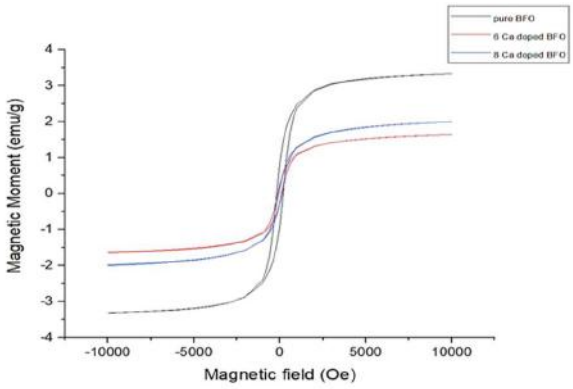

Figure 3: M-H curve of $BiFeO_3$, $Bi_{0.94}Ca_{0.06}FeO_3$ and $Bi_{0.92}Ca_{0.08}FeO_3$ annealed at 550°C for two hours of holding time.

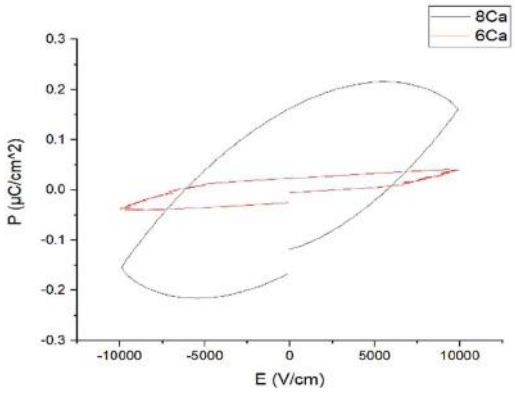

Figure 4: P-E curve of $Bi_{0.94}Ca_{0.06}FeO_3$ and $Bi_{0.92}Ca_{0.08}FeO_3$ sintered at 550°C for two hours of holding time.

3.4 Ferroelectric Measurement

The room temperature ferroelectric analysis was performed by Radiant Precision Multimeter using a frequency of 100 Hz and a maximum applied electric field of 10kV and the P-E loops are represented in Figure 4. Weak ferroelectric behavior with incomplete saturation was observed for the Ca-doped BFO powders. The P-E hysteresis loopsalso indicate that the leakage current characteristics increase with increasing %Ca. The remnant polarization (P_r) and the saturation polarization (P_s) was observed to increase with increasing percentage of doping. On the other hand, the coercive electric field was observed to decrease with increasing amount of dopant. The obtained data is tabulated in Table 3. The displacement of Bi ion and Fe-O octahedron is responsible for the ferroelectric nature of BFO. 8%Ca-doped BFO sample displays symmetric P-E hysteresis loops and it implies that, calcium could be responsible for the stabilization of domain walls which interact with vacancies (Costa *et al.,* 2015).

Table 3: Ferroelectric properties of pure and Ca-doped BFO

Sample Identity	E_c(V/cm)	P_r (μC/cm^2)	P_S (μC/cm^2)
$Bi_{0.94}Ca_{0.06}FeO_3$	2445.28	0.02258	0.04126
$Bi_{0.92}Ca_{0.08}FeO_3$	5654.35	0.16299	0.21579

4. CONCLUSIONS

Pure and Ca doped bismuth ferrite samples were synthesized using the sol-gel route. The XRD results exhibited slight displacement of the peaks due to Ca substitution, which indicate the change in lattice parameters of the samples. Rietveld refinement was conducted to find out the structure parameters and phase compositions of the samples. Since the amount of Ca substitution was limited to 8%, the substitution did not change the crystal structure. However, addition of excess bismuth nitrate at the initial stage of the process to compensate to the volatilization of Bi from BFO left some bismuth oxide residue in the samples. The FESEM results revealed that the particle size decreases with the substitution of Bi by Ca through formation of oxygen vacancies. The reduced particle size also has an effect of the magnetic property. The Ferroelectric P-E hysteresis loops of the Ca doped samples exhibit incomplete saturation of the hysteresis loops. The leakage current characteristics increase with increasing the %Ca which indicates towards the reduction in ferroelectric properties of Ca doped BFO.

ACKNOWLEDGEMENTS

The authors are grateful to the department of Materials and Metallurgical Engineering and the department of Glass and Ceramic Engineering at Bangladesh University of Engineering and Technology, and Atomic Energy Commission, Dhaka Center for providing laboratory facilities to conduct this research.

REFERENCES

Bhushan, B., Basumallick A., Vasanthacharya N., Kumar S., and Das D., 2010. Sr induced modification of structural, optical and magnetic properties in $Bi_{1-x}Sr_xFeO_3$ (x= 0, 0.01, 0.03, 0.05 and 0.07) multiferroic nanoparticles, Solid State Sci., **12**(7), 1063-1069.

Bhushan, B., Das D., Priyam A., Vasanthacharya N., and Kumar S., 2012. Enhancing the magnetic characteristics of $BiFeO_3$ nanoparticles by Ca, Ba co-doping, Mater. Chem. Phys., **135**(1), 144-149.

Catalan, G., Sardar K., Church N., Scott J., Harrison R., and Redfern S., 2009. Effect of chemical pressure on the magnetic transition of multiferroic Ca-$BiFeO_3$, arXiv preprint arXiv:0903.2976.

Catalan, G., and Scott J. F., 2009. Physics and applications of bismuth ferrite, Adv. Mater., **21**(24), 2463-2485.

Chauhan, S., Arora M., Sati P., Chhoker S., Katyal S., and Kumar M., 2013. Structural, vibrational, optical, magnetic and dielectric properties of $Bi_{1-x}Ba_xFeO_3$ nanoparticles, Ceram. Int., **39**(6), 6399-6405.

Chauhan, S., Kumar M., Chhoker S., Katyal S., and Singh M., 2016. Substitution driven structural and magnetic transformation in Ca-doped $BiFeO_3$ nanoparticles, RSC advances, **6**(49), 43080-43090.

Cheng, C.-J., Kan D., Lim S.-H., McKenzie W., Munroe P., Salamanca-Riba L., Withers R., Takeuchi I., and Nagarajan V., 2009. Structural transitions and complex domain structures across a ferroelectric-to-antiferroelectric phase boundary in epitaxial Sm-doped $BiFeO_3$ thin films, Physical Review B, **80**(1), 01410.

Cheng, S., Li M., Deng S., Bao S., Tang P., Duan W., Ma J., Nan C., and Zhu J., 2016. Manipulation of magnetic properties by oxygen vacancies in multiferroic $YMnO_3$, Adv. Funct. Mater., **26**(21): 3589-3598.

Cheong, S.-W., and Mostovoy M., 2007. Multiferroics: a magnetic twist for ferroelectricity, Nature materials, **6**(1),13

Costa, L., Rocha L., Cortés J., Ramirez M., Longo E., and Simões A., 2015. Enhancement of ferromagnetic and ferroelectric properties in calcium doped $BiFeO_3$ by chemical synthesis, Ceram. Int., **41**(8), 9265-9275.

Dai, H., Li T., Chen Z., Liu D., Xue R., Zhao C., Liu H., and Huang N., 2016. Studies on the structural, electrical and magnetic properties of Ce-doped $BiFeO_3$ ceramics, J. Alloys Compd., **672,** 182-189.

Dhir, G., Uniyal P., and Verma N., 2018. Multiferroic properties of Sr-doped $BiFeO_3$ nanoparticles, Physica B: Condensed Matter, **531**, 51-57.

Ederer, C., and Spaldin N. A., 2005. Weak ferromagnetism and magnetoelectric coupling in bismuth ferrite, Physical Review B, **71**(6), 060401.

Fiebig, M., Lottermoser T., Fröhlich D., Goltsev A. V., and Pisarev R. V., 2002. Observation of coupled magnetic and electric domains, Nature, **419**(6909), 818.

Gautam, A., Singh K., Sen K., Kotnala R., and Singh M., 2011. Crystal structure and magnetic property of Nd doped $BiFeO_3$ nanocrytallites, Mater. Lett., **65**(4), 591-594.

Han, Y., Mao W., Quan C., Wang X., Yang J., Yang T., Li X. A., and Huang W., 2014. Enhancement of magnetic and ferroelectric properties of $BiFeO_3$ by Er and transition element (Mn, Co) co-doping, Materials Science and Engineering: B, **188**, 26-30.

Huang, F., Lu X., Lin W., Wu X., Kan Y., and Zhu J., 2006. Effect of Nd dopant on magnetic and electric properties of $BiFeO_3$ thin films prepared by metal organic deposition method, Appl. Phys. Lett., **89**(24), 242914.

Huang, J.-Z., Shen Y., Li M., and Nan C.-W., 2011. Structural transitions and enhanced ferroelectricity in Ca and Mn co-doped $BiFeO_3$ thin films, J. Appl. Phys., **110**(9), 094106.

Khomchenko, V., Kiselev D., Vieira J., Jian L., Kholkin A., Lopes A., Pogorelov Y., Araujo J., and Maglione M., 2008. Effect of diamagnetic Ca, Sr, Pb, and Ba substitution on the crystal structure and multiferroic properties of the $BiFeO_3$ perovskite, J. Appl. Phys, **103**(2), 024105.

Khomchenko, V., Kopcewicz M., Lopes A., Pogorelov Y., Araujo J., Vieira J., and Kholkin A., 2008. Intrinsic nature of the magnetization enhancement in heterovalently doped $Bi_{1-x}A_xFeO_3$ (A= Ca, Sr, Pb, Ba) multiferroics, J. Phys. D: Appl. Phys., **41**(10), 102003.

Kimura, T., Goto T., Shintani H., Ishizaka K., Arima T.-H., and Tokura Y., 2003. Magnetic control of ferroelectric polarization, nature, **426**(6962), 55.

Koval, V., Skorvanek I., Durisin J., Viola G., Kovalcikova A., Svec P., Saksl K., and Yan H., 2017. Terbium-induced phase transitions and weak ferromagnetism in multiferroic bismuth ferrite ceramics, Journal of Materials Chemistry C, **5**(10), 2669-2685.

Kumar, M. M., Palkar V., Srinivas K., and Suryanarayana S., 2000. Ferroelectricity in a pure $BiFeO_3$ ceramic, Appl. Phys. Lett., **76**(19), 2764-2766.

Kumar, P., and Kar M., 2014. Effect of Structural Transition on Magnetic Properties of Ca and Mn co-substituted $BiFeO_3$ Ceramics, arXiv preprint arXiv:1401.4059.

Lahmar, A., Habouti S., Dietze M., Solterbeck C.-H., and Es-Souni M., 2009. Effects of rare earth manganites on structural, ferroelectric, and magnetic properties of $BiFeO_3$ thin films, Appl. Phys. Lett., **94**(1), 012903.

Lee, D., Kim M. G., Ryu S., Jang H. M., and Lee S. G., 2005. Epitaxially grown La-modified $BiFeO_3$ magnetoferroelectric thin films, Appl. Phys. Lett., **86**(22), 222903.

Lin, J., Guo Z., Li M., Lin Q., Huang K., and He Y., 2018. Magnetic and dielectric properties of Ca-substituted $BiFeO_3$ nanoferrites by the sol-gel method, J. Appl. Biomater. Funct. Mater.,**16**(1_suppl), 93-100.

Liu, J., Li M., Pei L., Wang J., Yu B., Wang X., and Zhao X., 2010. Structural and multiferroic properties of the Ce-doped $BiFeO_3$ thin films, J. Alloys Compd., **493**(1-2), 544-548.

Makhdoom, A., Shah S. M., Mahmood T., Iqbal M. J., Akhtar M., and Rafiq M., 2019. Enhancement of ferromagnetism by suppression of spiral spin structure in Ba doped $BiFeO_3$, J. Magn. Magn. Mater., **484**, 286-290.

Manz, S., Matsubara M., Lottermoser T., Büchi J., Iyama A., Kimura T., Meier D., and Fiebig M., 2016. Reversible optical switching of antiferromagnetism in $TbMnO_3$, Nature Photonics, **10**(10), 653.

Martin, L., Crane S., Chu Y., Holcomb M., Gajek M., Huijben M., Yang C.-H., Balke N., and Ramesh R., 2008. Multiferroics and magnetoelectrics: thin films and nanostructures, J. Phys.: Condens. Matter, **20**(43), 43422

Marzouk, M., Hashem H., Soltan S., and Ramadan A., 2020. Room temperature ferromagnetism driven by Ca-doped $BiFeO_3$ multiferroic functional material, Journal of Materials Science: Materials in Electronics, 1-9.

Masó, N., and West A. R., 2012. Electrical properties of Ca-doped $BiFeO_3$ ceramics: from p-type semiconduction to oxide-ion conduction, Chem. Mater., **24**(11), 2127-2132.

Pattanayak, S., Choudhary R., Shannigrahi S., Das P. R., and Padhee R., 2013. Ferroelectric and ferromagnetic properties of Gd-modified $BiFeO_3$, J. Magn. Magn. Mater., 341, 158-164.

Qi, X., Dho J., Tomov R., Blamire M. G., and MacManus-Driscoll J. L., 2005. Greatly reduced leakage current and conduction mechanism in aliovalent-ion-doped $BiFeO_3$, Appl. Phys. Lett., **86**(6), 062903.

Ramesh, R., 2014. Electric field control of ferromagnetism using multi-ferroics: the bismuth ferrite story,Philos. Trans. Royal Soc. A, 372(2009), 20120437.

Sayedaghaee, S. O., Xu B., Prosandeev S., Paillard C., and Bellaiche L.,2019. Novel dynamical magnetoelectric effects in multiferroic $BiFeO_3$, Phys. Rev. Lett., **122**(9), 097601.

Seshadri, R., and Hill N. A., 2001. Visualizing the role of Bi 6s "lone pairs" in the off-center distortion in ferromagnetic $BiMnO_3$, Chem. Mater., **13**(9), 2892-2899.

Soltani, T., and Lee B.-K., 2016. Novel and facile synthesis of Ba-doped $BiFeO_3$ nanoparticles and enhancement of their magnetic and photocatalytic activities for complete degradation of benzene in aqueous solution, J. Hazard. Mater., 316, 122-133.

Sosnowska, I., Neumaier T. P., and Steichele E., 1982. Spiral magnetic ordering in bismuth ferrite, Journal of Physics C: Solid State Physics, **15**(23), 4835.

Tahir, M., Riaz S., Khan U., Hussain S. S., Nairan A., Akbar A., Saleem M., Atiq S., and Naseem S., 2020. Enhanced structural and magnetic ordering in as-synthesized Ca doped bismuth iron oxide nanoceramics, J. Alloys Compd., 832, 154725.

Troyanchuk, I., Bushinsky M., Karpinsky D., Mantytskaya O., Fedotova V., and Prochnenko O., 2009. Structural transformations and magnetic properties of Bi_{1-x} Ln_x FeO_3 (Ln= La, Nd, Eu) multiferroics, physica status solidi (b), **246**(8), 1901-1907.

Van Aken, B. B., Palstra T. T., Filippetti A., and Spaldin N. A., 2004. The origin of ferroelectricity in magnetoelectric $YMnO_3$, Nature materials, **3**(3), 164.

Wang, D., Goh W., Ning M., and Ong C., 2006. Effect of Ba doping on magnetic, ferroelectric, and magnetoelectric properties in mutiferroic $BiFeO_3$ at room temperature, Appl. Phys. Lett., **88**(21), 212907.

Wang, J., Neaton J., Zheng H., Nagarajan V., Ogale S., Liu B., Viehland D., Vaithyanathan V., Schlom D., and Waghmare U., 2003. Epitaxial $BiFeO_3$ multiferroic thin film heterostructures, Science, **299**(5613), 1719-1722.

Wang, K., Liu J.-M., and Ren Z., 2009. Multiferroicity: the coupling between magnetic and polarization orders, Adv. Phys., **58**(4), 321-448.

Wang, T., Wang X.-L., Song S.-H., and Ma Q., 2020. Effect of rare-earth Nd/Sm doping on the structural and multiferroic properties of $BiFeO_3$ ceramics prepared by spark plasma sintering, Ceram. Int.

Wang, X., Wang S., Liu W., Xi X., Zhang H., Guo F., Xu X., Li M., Liu L., and Zhang C., 2015. Novel electrical conductivity properties in Ca-doped $BiFeO_3$ nanoparticles, J. Nanopart. Res., **17**(5), 209.

Wang, Y., and Nan C.-W.,2008. Effect of Tb doping on electric and magnetic behavior of $BiFeO_3$ thin films, J. Appl. Phys., **103**(2), 024103.

Xiang, H., Wei S.-H., Whangbo M.-H., and Da Silva J. L., 2008. Spin-orbit coupling and ion displacements in multiferroic $TbMnO_3$, Phys. Rev. Lett., **101**(3), 037209.

Yang, C.-H., Seidel J., Kim S., Rossen P., Yu P., Gajek M., Chu Y.-H., Martin L. W., Holcomb M., and He Q., 2009. Electric modulation of conduction in multiferroic Ca-doped $BiFeO_3$ films, Nature materials, **8**(6), 485.

Yoneda, Y., Yoshii K., Saitoh H., and Mizuki J., 2007. Magnetic and Ferroelectric Properties of $(Bi_{1-x}La_x)FeO_3$, Ferroelectrics, **348**(1), 33-37.

Yotburut, B., Thongbai P., Yamwong T., and Maensiri S., 2017. Electrical and nonlinear current-voltage characteristics of La-doped $BiFeO_3$ ceramics, Ceram. Int., **43**(7), 5616-5627.

Yu, B., Li M., Liu J., Guo D., Pei L., and Zhao X., 2008. Effects of ion doping at different sites on electrical properties of multiferroic $BiFeO_3$ ceramics, J. Phys. D: Appl. Phys., **41**(6): 065003.

Yuan, G., Or S. W., Liu J., and Liu Z., 2006. Structural transformation and ferroelectromagnetic behavior in single-phase $Bi_{1-x}Nd_xFeO_3$ multiferroic ceramics, Appl. Phys. Lett., **89**(5), 052905.

Zhai, L.-J., and Wang H.-Y., 2017. The magnetic and multiferroic properties in $BiMnO_3$, J. Magn. Magn. Mater., 426, 188-194.